HIGH SCHOOL EDITION
Journal of Student Research
Volume 14 Issue 1 (2025)

Bamboo Spine

Jayveer Kochhar[1] and Vinay Vishwakarma[#]

[1]Omtec, India
[#]Advisor

ABSTRACT

The most prevalent forms of SpA in the US are AS and non-radiographic axial SpA, which together have a prevalence of 0.7% to 1.4%. A class of autoimmune diseases known as seronegative spondyloarthropathies (SSA) causes normal body cells to assault the musculoskeletal system, resulting in unstable, fracture-prone weak joints in the bones. Millions of people worldwide struggle with this issue, which is also one of the most difficult to identify and manage. This is because more than basic tests or a visit to the doctor is often needed to identify the diagnosis, which frequently calls for complicated scans. These spine issues can result in rib cage congestion, which alters breathing patterns and causes chest expansions in various places of the torso. In the group of autoimmune diseases known as seronegative spondyloarthropathies (SSA), normal body cells attack the cells in our musculoskeletal system, causing the weak joints in our bones to become unstable and brittle. These spine issues also result in rib cage congestion, which alters breathing patterns and causes chest expansions in various thoracic regions. Five force-sensitive resistors are used in total by our prototype approach. These are fastened to a belt that encircles your whole chest, mapping the chest's growth and mobility in every dimension. This information is used to calculate the chest's expansion, including its size, rate, and force. An IMU sensor will be used in the project to measure the chest's movement. The device's microcontroller will receive all of this data and forward it to a wireless communication module. Data will be sent by this wireless connection module to a phone or laptop so that it may be processed. We may use the second derivative of the acceleration to calculate the distance traveled or the expansion of the chest. We will need to perform a Riemann sum twice to determine the distance because our data is discrete rather than continuous. We may multiply the value by the interval between readings to determine the velocity at a specific moment.

Introduction

Seronegative Inflammatory arthritis conditions affecting the spine and sacroiliac joints are known as spondyloarthropathies (SSA). Because they do not test positive for RF, an antibody associated with rheumatoid arthritis, they are referred to as "seronegative". Ankylosing spondylitis, reactive arthritis, psoriatic arthritis, and inflammatory bowel disease account for the majority of instances of SSA. Breathing is slowed by spinal abnormalities brought on by ankylosing spondylitis, one kind of SSA. As inflammation grows, the spine stiffens and fuses together. This may limit the range of motion in the chest, making it more difficult to expand and breathe deeply. Breathing difficulties may arise from ankylosing spondylitis due to interrelated reasons. Spinal fusion, which reduces chest expansion while breathing and compromises rib joints and spine movement, is brought on by chronic inflammation. Restrictive lung disease keeps the lungs from fully expanding because of diminished TLC and VC. A stiff chest wall can hinder the diaphragm's ability to operate, which increases breathing, exhaustion, and dyspnea by requiring the recruitment of auxiliary muscles for inhalation.

Some individuals get pleuritis and lung fibrosis, which further narrows the airways. Because of the structure or function of the upper airways, ankylosing spondylitis has been related in certain studies to obstructive sleep apnea. The intricate connection between the respiratory and musculoskeletal systems, as well as the systemic effect of Seronegative Spondyloarthropathies on health, are highlighted by these aspects. Chest expansion, a straightforward and

non-intrusive measurement of chest expansion during deep breathing, is essential for the early identification of ankylosing spondylitis. A markedly diminished expansion of the chest in relation to normal values could indicate seronegative spondyloarthropathies. The proposed device detects chest displacement at five places and is a portable chest expansion measurement tool based on an IMU.

Methods

The rib cage is a moving organ. It can increase and shrink with your lungs. Like other bones present in the body, it can thin with age. Gradual bone loss causes your ribs to lose some of their bulk. A study published in ASME Proceedings, the ribs also become calcified along with age which means the bones lose their flexibility and break. X-ray scans show that the calcification has increased from 6% in a person who is in their 30s and 45% when the person is in their 90s.

Ribcage bones become thinner and change shape, which alters the ribcage so that it expands very little and contracts while breathing. The nerves in the airways that trigger coughing become less sensitive to foreign particles. When particles build up in the lungs, they can damage the lung tissue. A minimal increase in the rib cage size is seen from age 20 to 30 while it appears fairly constant for ages 30-100.The rib cage shape changes along with age which is quite visible, particularly for the angle of the ribs relative to the spine and the kyphosis of the spine. As people age, their chest wall stiffness and thorax shape alter as a result of dorsal kyphosis/anteroposterior diameter (also known as "barrel chest"), calcification of the costal cartilages, and narrowing of intervertebral gaps. It makes sense to anticipate that the lungs will undergo morphological changes concurrent with the thorax, given their close proximity to one another.

In women who are not in long-term care their chest wall mobility at the axillary level and respiratory function decreased. Increasing chest wall stiffness and changes to thorax shape due to calcification of costal cartilages, tapering of intervertebral spaces, and increased dorsal kyphosis/anteroposterior diameter (‘barrel chest’)is associated with advancing age, given the tight positions of the lungs and the chest wall, it is reasonable to expect that the lung changes its shape along with the thorax.

How Are Chest Movements Affected During Rib Fractures

Paradoxical movement of a portion of the chest wall is the most common symptom - that is the affected area goes in when the patient breathes in and the rest of the chest expands, as the patient exhales the affected area moves outwards and the rest of the chest contracts. The flail chest slides inside during the inspiration while the ribs move outward; the converse happens during the expiration. We refer to this as paradoxical motion. Blunt trauma to the thorax, including direct strikes, falls from a height, and automobile accidents, is frequently the cause of a flail chest.

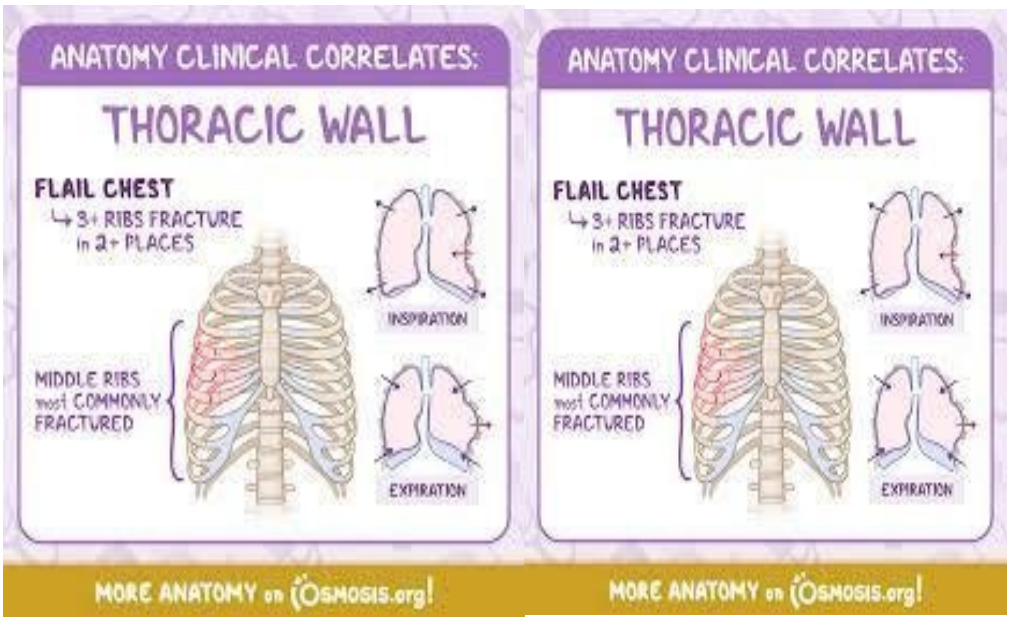

Figure 2. Anatomy Clinical Correlates

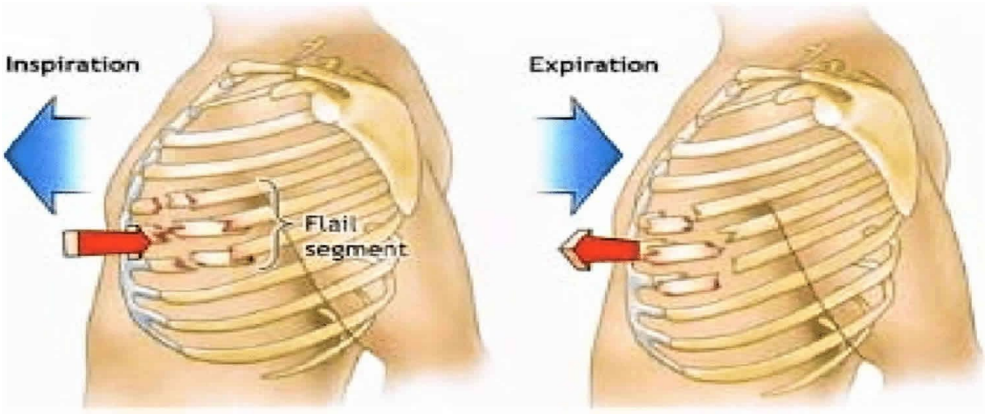

Figure 3. Flail Segment: Inspiration, Expiration

Chest movements affected in diseases like lungs or COPD?

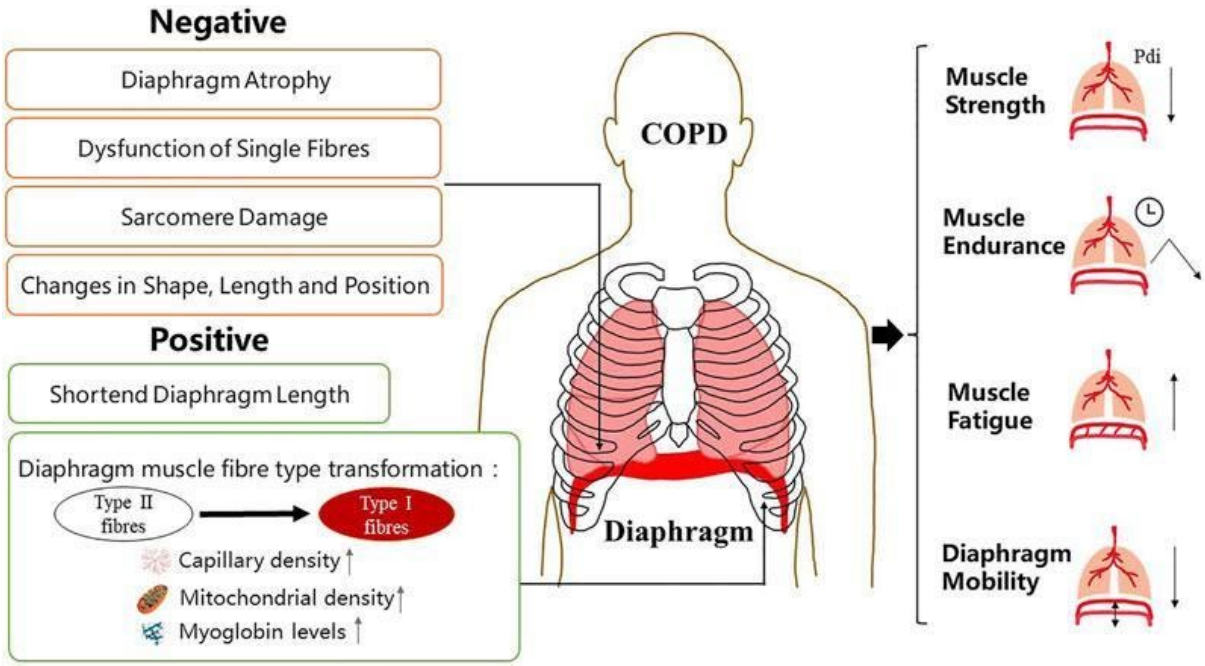

5-12 years is 2nd Intercostal space- 1 inch/ 2.5 cm,
4th Intercostal space- 1 inch/2.5 cm,
6th Intercostal space- 1.7 inch/ 4.25cm.

Figure 4. Chest movements

Distance Calculation With IMU

BNO055 can provide linear acceleration (Acceleration along individual axes of IMU) along with Gravity Vector in the Fusion mode. We can use the linear acceleration data to calculate the displacements occurring along the different axes of the IMU. Displacement along an axis can be found by double integrating the acceleration values.

$$d_c(t) = d_0 + v_0 t + \int_0^t dt \int_0^\tau a(\tau) d\tau$$

The above formula can be used to calculate the displacement values from the acceleration data. But the formula is only valid for continuous functions. The acceleration data provided by IMU is discrete. So we use trapezoidal integration to calculate the displacement. Below figure illustrates the simple trapezoidal method, where the region under the analog signal is approximated by the sum of a series of rectangles. The time increment between samples Δt depends on the measurement sampling frequency, in other words it depends on how often the analog signal a(t) is digitalized. The Δt step must be small enough to approximate signals with "high curvature" minimizing the calculation error. This means that the sampling frequency should be high enough in relation to the highest frequency content of the waveform. We can get 100HZ acceleration data output from BNO055 IMU.

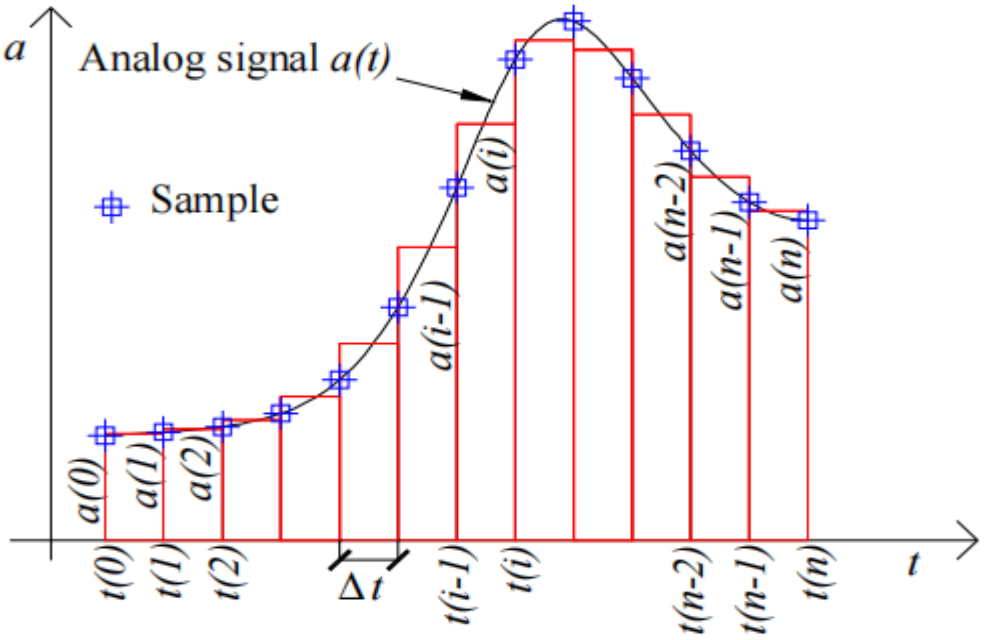

Figure 5. Trapezoidal Integration graph

Once we have the data in a discrete-time domain, we can use trapezoidal integration to calculate the velocity and displacement.

$$\int_{t(0)}^{t(n)} a(t)dt \cong \sum_{i=1}^{n}\left(\frac{a(i-1)+a(i)}{2}\right)\Delta t$$

where:
a (t): continuous time domain waveform
a(i): *i th* sample of the time waveform
Δt : time increment between samples (*t(i)-t(i-1)*)
n: number of samples of the digital record

Thus, displacements can be calculated recursively in two steps, first, computing velocity from acceleration, and then, computing displacement from velocity:

$$v_c(i) = v_c(i-1) + \frac{a(i-1)+a(i)}{2}\Delta t$$

$$d_c(i) = d_c(i-1) + \frac{v(i-1)+v(i)}{2}\Delta t$$

where:
a (i): *i th* sample of the acceleration waveform
vc (i): *i th* sample of the calculated velocity
dc (i): *i th* sample of the calculated displacement

Before we do the integration of IMU's linear acceleration data we need to find the quaternion that will rotate the linear acceleration vector to align it with the global frame. This is important because the IMU when mounted on the show or any body part is not aligned with the global frame because of the curvature of the surface. This makes it important for IMU readings to be tilt-compensated for the data to make sense. So every IMU reading is rotated to align with the global frame. The below steps define the methods used to align the z-axis of the IMU with the global Z-axis (gravity vector). Similar steps can be incorporated to align other axes as well.

qi = [wi ,xi ,yi ,zi] Quaternion reading for the i^{th} reading

Lai=[Lzi,Lzi,Lzi] Linear acceleration of the i^{th} reading

Now to determine the quaternion about which to rotate the vector we can use matrix multiplication of the quaternions(IMU's z-axis with the gravity vector which is aligned with the global z-axis)

Gz = [0 , 0 , 1] Gravity vector

After determining the angle and the vector we can get the calibration quaternion which will rotate the Linear acceleration vector to align with the global frame. The below formula can be used to determine the calibration quaternion. The first component in the matrix is the scalar component of the quaternion and the second is the vector.

$$\boldsymbol{q}(\theta,\ \boldsymbol{n}) = (\cos(\frac{\theta}{2}), \boldsymbol{n}\sin(\frac{\theta}{2})).$$

n= [xi ,yi ,zi]
= [wi]
Once we have the calibration quaternion, we can use the quaternion multiplication to rotate the vector.

La-corr-i = qcalib-i * La-i * qcalib-i-1

where :
La-corr-i - Corrected linear acceleration data
qcalib-i - Calibration quaternion
La-i - Linear acceleration
qcalib-i-1 - Inverse of calibration quaternion

All the above calculations are repeated for all the IMU data points.

To validate the effectiveness of the above calculations we can cross-check the gravity vector graph. Making sure the Z axis always has approximately 9.8m/s^2. The graph below shows gravity vectors along the z-axis before and after applying the calibration.

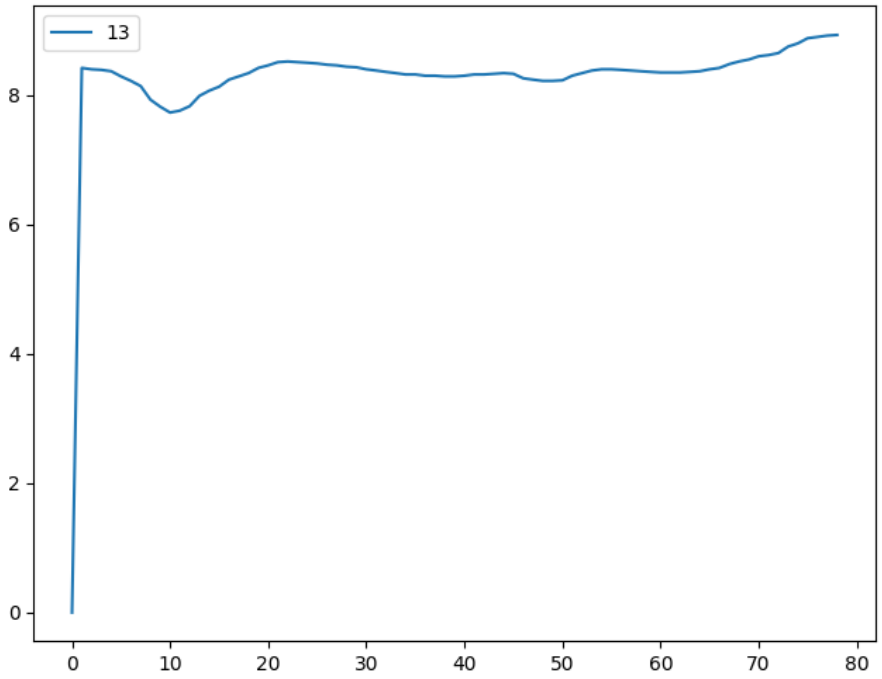

Figure 6. Raw Gravity vector data along z axis

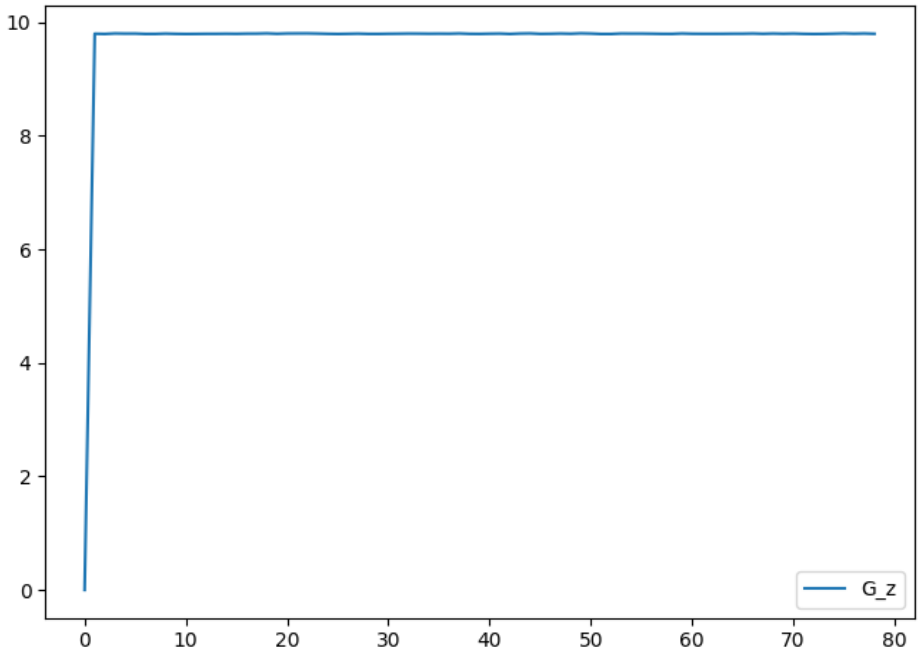

Figure 7. Tilt-compensated Gravity data

From the above images, it is clear that the proposed method aligns the z-axis of the IMU with the global z axis. The same steps are repeated for one of the other axis which aligns the entire IMU in the direction of the reference

frame. Once the IMU is aligned, we can calculate the displacement for a single IMU unit below is the calculation for 4 IMUs working together.

1. Define Variables:

xi, yi, zi 3D coordinates of IMU i, where i=1, 2, 3, 4

xi,yi, zi : Roll, pitch, and yaw angles for IMU i

dxi,dyi, dzi : Displacement in the x, y, and z directions for IMU i

2. Orientation Transformation:

As stated above, the Orientation will be required same can be given by the below formula:

Lf = q * Li * q-1=

3. Calculate Displacement:

The displacement in each direction can be calculated using the difference in coordinates between time points:

$$d_{xi} = x_i(t_2) - x_i(t_1)$$
$$d_{yi} = y_i(t_2) - y_i(t_1)$$
$$d_{zi} = z_i(t_2) - z_i(t_1)$$

4. Combine Data from All IMUs:

To combine the data from all four IMUs to calculate the overall displacement of the chest in each direction. This could be done by using a weighted average because the IMUs are not symmetrically placed.

$$D_x = \frac{d_{x1} + d_{x2} + d_{x3} + d_{x4}}{4}$$
$$D_y = \frac{d_{y1} + d_{y2} + d_{y3} + d_{y4}}{4}$$
$$D_z = \frac{d_{z1} + d_{z2} + d_{z3} + d_{z4}}{4}$$

Figure 8. Prototype CAD design

Figure 9. Prototype front view

Assessment of chest expansion was done using CTM at three landmarks

1. upper [2nd intercostal space],
2. middle [4th intercostal space]
3. lower [xiphoid] chest).

The anatomical markers used to define upper chest expansion were the third intercostal space at the level of the clavicular line spinous processes of the fifth thoracic vertebrae.

Follow the images

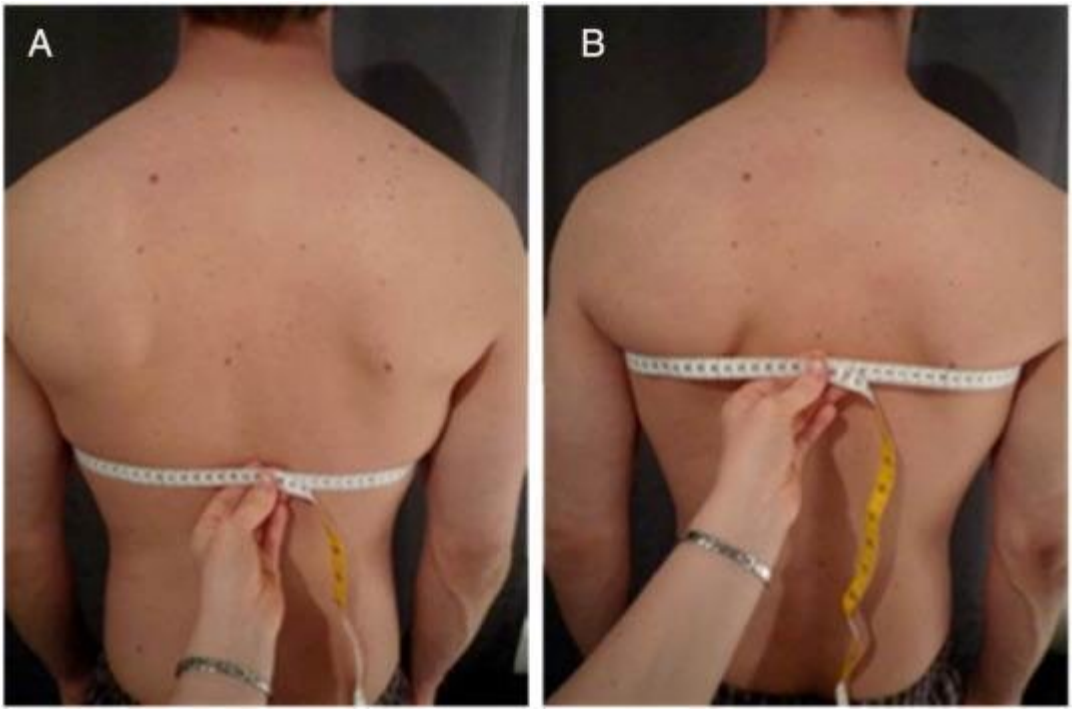

Figure 10a, 10b & 10c. CTM Landmarks

Sr. No.	Level	Females (n=293)		Males (n=283)	
		Mean (in Inches)	Std. Dev. (in Inches)	Mean (in Inches)	Std. Dev (in Inches)
1	2^{nd} ICS	2.22	0.76	2.76	0.9
2	4^{th} ICS	2.22	0.73	2.71	0.83
3	Zyphoid Process	2.27	0.78	2.99	0.87

Table 2. Gender-wise comparison of Chest Expansion

Observation

To calculate the displacement in the chest while breathing in all four directions the device is equipped with 4 IMUs to calculate the displacement which was rigorously tested on a healthy person. The observations consist of 33 different time points for capturing the data for a complete breathing cycle. The chest movement in all three dimensions(x,y,z) for all IMUs where captured by the device accurately displaying a pattern consistent with normal and healthy breathing. The readings across the IMUs were consistent and reflected the symmetrical nature of chest movement in a healthy individual, demonstrating the device's reliability. The sensitivity of the device allowed it to detect even the subtle changes in the chest displacement, charting the entire breathing pattern, including transitions. The observed pattern was in line with physiological expectations for a fit person, reflecting a smooth, sinusoidal-like motion typical of unlabored breathing. Furthermore, the successful capture of detailed breathing data, along with the robustness of the mathematical model, suggests that this device may have potential applications in clinical settings.

It could be useful in monitoring breathing patterns, detecting anomalies, or assisting in the diagnosis of conditions such as Seronegative Spondyloarthropathies

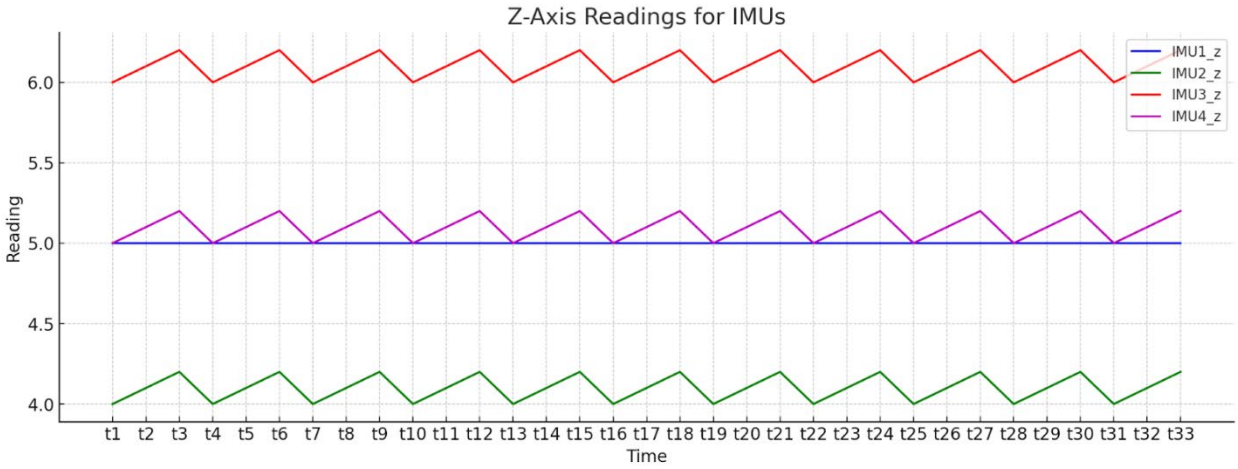

Figure 11. Z-Axis readings for IMU

Results

The prototype is not only a non-invasive but also a reusable device. The given solution differentiates and accurately predicts the chest movements for ankylosing spondylitis only and does not misdiagnose for other conditions such as chest deformities, obstructive bronchitis, etc. The device will help in the early diagnosis of ankylosing spondylitis which is quite challenging. This will restrict patients from other activities that may worsen the condition further such as scuba diving, high-altitude hiking, and other activities that require focus on breathing and chest expansion.

Discussion

Computer-aided design or CAD design is the process of creating, modifying, analyzing, or optimizing a design using computer software. I obtained practical experience with CAD programs including AutoCAD, SolidWorks, and Fusion 360 during the assignment. I gained knowledge about how to make intricate 3D models by comprehending the limits and geometry of the pieces I was designing. I also improved my ability to draft precise technical drawings that include material specifications, measurements, and assembly guidelines. Additionally, I learned how to run simulations to evaluate a design's robustness, performance, and endurance under various scenarios. Another important component was having a basic understanding of design concepts, such as ergonomics, usefulness, and aesthetics.

As I worked on design projects that required sharing and integrating various components developed by team members, collaboration was an essential component of the process. In addition, I improved my abilities to manage and arrange CAD files, including version control and paperwork.

Conclusion

The device's ability to understand complex breathing patterns was confirmed by the four inertial measurement units (IMUs), all of which continuously produced accurate and responsive data. Given its apparent efficacy, this method has great promise for improving health monitoring in a variety of non-clinical and clinical settings. It may also be

further improved to allow for the monitoring and diagnosis of certain diseases, including seronegative spondyloarthropathies. The initial testing seems promising, but there are still a number of issues that need to be resolved for further development, such as calibration, long-term stability, and usability. It may be possible to significantly improve the accuracy of the device by integrating it with additional sensor technologies or by applying sophisticated machine learning techniques. It is critical to thoroughly address ethical and regulatory issues, such as patient permission and data protection, as the technology moves closer to clinical deployment. By continuing research and working with specialists in specialized domains like pulmonology and biomechanics, the device's full potential may be achieved. A system's ability to be successfully tested not only confirms that it works as intended, but it also opens up possibilities for other uses, such as early diagnosis, therapeutic monitoring, and assistance with rehabilitation. When this technology moves from its experimental stage to practical use, engineers, doctors, and regulators will all need to be involved and cooperative in order for it to have a substantial impact on healthcare and general well-being.

Acknowledgments

I sincerely thank all of the instructors and mentors at On My Own Technology Pvt. Ltd. for assisting with this specific project. They have made it possible for me to carry out the research. I will always be appreciative of their assistance and kindness.

References

1. Li, Shilei, et al. "Multi-kernel Correntropy-based Orientation Estimation of IMUs: Gradient Descent Methods." IEEE Transactions on Instrumentation and Measurement (2023).
2. Laidig, Daniel and Thomas Seel. “VQF: Highly Accurate IMU Orientation Estimation with Bias Estimation and Magnetic Disturbance Rejection.” Inf. Fusion 91 (2022): 187-204.
3. Hao, Heng et al. “Highly Efficient Representation and Active Learning Framework for Imbalanced Data and its Application to COVID-19 X-Ray Classification.” ArXiv abs/2103.05109 (2021): n. Pag.
4. Liu, Wenxin et al. “TLIO: Tight Learned Inertial Odometry.” IEEE Robotics and Automation Letters 5 (2020): 5653-5660.
5. D. Roetenberg, H. Luinge and P. Veltink, "Inertial and magnetic sensing of human movement near ferromagnetic materials," The Second IEEE and ACM International Symposium on Mixed and Augmented Reality, 2003. Proceedings., Tokyo, Japan, 2003, pp. 268-269, doi: 10.1109/ISMAR.2003.1240714. keywords: {Magnetic materials;Gyroscopes;Magnetic separation;Accelerometers;Magnetic field measurement;Magnetometers;Magnetic sensors;Magnetic flux;Filters;Signal design},
6. Harper BE, Reveille JD. Spondyloarthritis: clinical suspicion, diagnosis, and sports. Curr Sports Med Rep. 2009 Jan-Feb;8(1):29-34. doi: 10.1249/JSR.0b013e3181967ac6. PMID: 19142077; PMCID: PMC2898732.
7. Parwata, I. Made Yoga et al. “Correlation between the mobility of the above cage and the below thorax cage toward the elderly lung vital capacity.” Bali Medical Journal (2021): n. pag.
8. Fisher LR, Cawley MI, Holgate ST. Relation between chest expansion, pulmonary function, and exercise tolerance in patients with ankylosing spondylitis. Ann Rheum Dis. 1990 Nov;49(11):921-5. doi: 10.1136/ard.49.11.921. PMID: 2256739; PMCID: PMC1004263.
9. Yazgan Ç, Ertürk H, Taşkın A. Imaging Features of Thoracic Manifestations of Behçet's Disease: Beyond Pulmonary Artery Involvement. Curr Med Imaging. 2021;17(8):996-1002. doi: 10.2174/1573405617999210112193856. PMID: 33438546; PMCID: PMC8653419.
10. Dhahri R, Mejri I, Ghram A, Dghaies A, Slouma M, Boussaid S, Metoui L, Gharsallah I, Ayed K, Moatemri Z, Farahat RA, AlHamdani A, Dergaa I. Assessment Tools for Pulmonary Involvement in Patients with Ankylosing Spondylitis: Is Diaphragmatic Ultrasonography Correlated to Spirometry? J

Multidiscip Healthc. 2023 Jan 11;16:51-61. doi: 10.2147/JMDH.S393061. PMID: 36660040; PMCID: PMC9843477.

11. Maria Ragnarsdottir, Arni Jon Geirsson, Bjorn Gudbjornsson, Rib cage motion in ankylosing spondylitis patients: a pilot study, The Spine Journal, Volume8, Issue3,2008, Pages505-509, ISSN 1529-9430,https://doi.org/10.1016/j.spinee.2006.12.009.(https://www.sciencedirect.com/science/article/pii/S1529943007000006X)